J|A|C|S COMMUNICATIONS

Published on Web 07/24/2009

Reaction Regimes on the Synthesis of Hollow Particles by the Kirkendall Effect

Andreu Cabot,*,† Maria Ibáñez,† Pablo Guardia,† and A. Paul Alivisatos‡

Departament d'Electrònica and Institut de Nanociència i Nanotecnologia, Universitat de Barcelona, Barcelona 08028, Spain, Department of Chemistry, University of California at Berkeley, and Materials Sciences Division, Lawrence Berkeley National Laboratory, Berkeley, California 94720

Received May 13, 2009; E-mail: acabot@ub.edu

In the simplest scenario, the synthesis of hollow nanostructures by the Kirkendall effect involves the reaction of solid particles of composition A, with an element B in solution or gas phase, to form AB nanostructures. When the reaction front localizes at the AB/B interface, the outward diffusion of the core element A through the growing AB composite generates a cavity inside the particle. Since the initial report in 2004,[1] such a mechanism has been applied to the synthesis of hollow nanostructures from a plethora of materials, including oxides, phosphides, and chalcogenides.[2] In previous reports, it is usually assumed that hollow particles are obtained only if and when the self-diffusivity through the AB shell is larger for the core element A than for the external element B.[3] In the present communication, we show that the reaction of identical A−B couples can lead to different particle geometries depending on the reaction conditions. We explain such a product disparity from reactions involving the diffusion of equal species through an identical composite, in terms of the concentration and reactivity of the anion precursor.

Solid cadmium particles were synthesized in solution by injecting dimethylcadmium (0.1 mL, 97%, Strem) with trioctylphosphine (1 mL, TOP, 97%, Strem) into trioctylphosphine oxide (10 g, TOPO, 99% Arcos) at 330 °C.[4] The reaction of the spherical Cd crystals obtained by this procedure with the chalcogens is performed by injecting the selected chalcogen precursor into the heated solution containing the Cd particles. The chalcogen precursor solutions were prepared in an argon-filled glovebox by dissolving S, Se, or Te (>99.998%, Aldrich) in TOP, and S in anhydrous 1,2-dichlorobenzene (DCB, 99%, Aldrich), to form the complexes TOPS, TOPSe, TOPTe, and the molecular solution DCB:S.

The complete reaction of Cd particles with a large excess of DCB:S at $T \approx 250$ °C takes place in ~20 min and results in hollow CdS particles with spherical geometry and large inner-to-outer radius ratios: $R_I/R_O = 0.65 \pm 0.02$ (Figure 1A).[4,5] On the other hand, the complete reaction of Cd particles with TOPS at $T \approx 250$ °C requires over 20 h and leads to the formation of solid CdS particles with spherical geometry (Figure 1C). At $T \approx 310$ °C, the same reaction results in asymmetric CdS particles (Figure 1D). In parallel, the reaction of Cd particles with a large excess of TOPSe results in hollow CdSe particles having $R_I/R_O = 0.5 \pm 0.1$ (Figure 1B). However, solid CdSe particles are produced from the reaction of Cd particles with a low TOPSe concentration ([TOPSe]/[Cd] ≈ 1) (Figure 1E).

We use a kinetic model of the particle oxidation reaction to simulate the growth of hollow particles. In the reaction of A particles with an element B in solution, to form an AB shell, the inside and outside radius variations are determined by the number of reactions at the A/AB and AB/solution interfaces: $N_{A/AB}$ and $N_{AB/S}$, respectively. The reaction frequency at each interface depends on the diffusion time of both elements through the shell, the collision frequency, and the reaction probability:

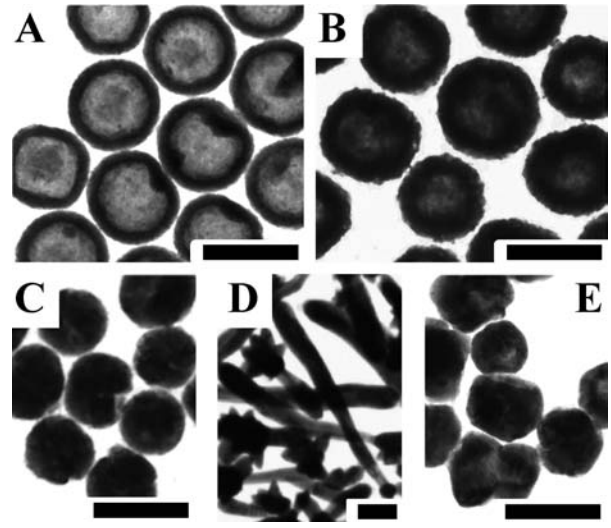

Figure 1. TEM micrographs of the products of the reaction of spherical Cd particles with: (A) DCB:S, [S]/[Cd] ≈ 8, $T = 250$ °C; (B) TOPSe, [Se]/[Cd] ≈ 8, $T = 250$ °C; (C) TOPS, [S]/[Cd] ≈ 8, $T = 250$ °C; (D) TOPS, [S]/[Cd] ≈ 8, $T = 310$ °C; (E) TOPSe, [Se]/[Cd] ≈ 1, $T = 250$ °C. All scale bars correspond to 400 nm.

$$R_{I_{i+1}} = \left(R_{I_i}^3 - \frac{3}{4\pi}\frac{N_{A/AB}FW}{\rho L}\right)^{1/3};\ N_{A/AB} = IP_{r_{A/AB}}P_T\theta_B$$

$$R_{O_{i+1}} = \left(R_{O_i}^3 + \frac{3}{4\pi}\frac{N_{AB/S}FW}{\rho L}\right)^{1/3};\ N_{AB/S} = IP_{r_{AB/S}}\theta_A$$

where R_{I_i} and R_{O_i} are the inside and outside radius of the shell at iteration i. FW, ρ, and L are the formula weight and density of AB and Avogadro's number, respectively. I is the collision frequency of B with the particle surface, which depends on the temperature, solvent viscosity, B concentration, and A particle size. $P_{r_{A/AB}}$ and $P_{r_{AB/S}}$ are the probabilities of reaction at the A/AB and AB/solution interfaces, respectively. P_T is the probability for an impending B molecule to be trapped and diffuses inside AB. Finally, θ_B and θ_A are the probabilities that, at a given time, the trapped B ions/molecules reach the A/AB interface and that the A ions reach the AB/solution interface, respectively. These probabilities depend on the comparison between the ion self-diffusion and the shell growth rate. We approximate them to be 1 when the diffusion time across

† Universitat de Barcelona.
‡ University of California at Berkeley and Lawrence Berkeley National Laboratory.

10.1021/ja903751p CCC: $40.75

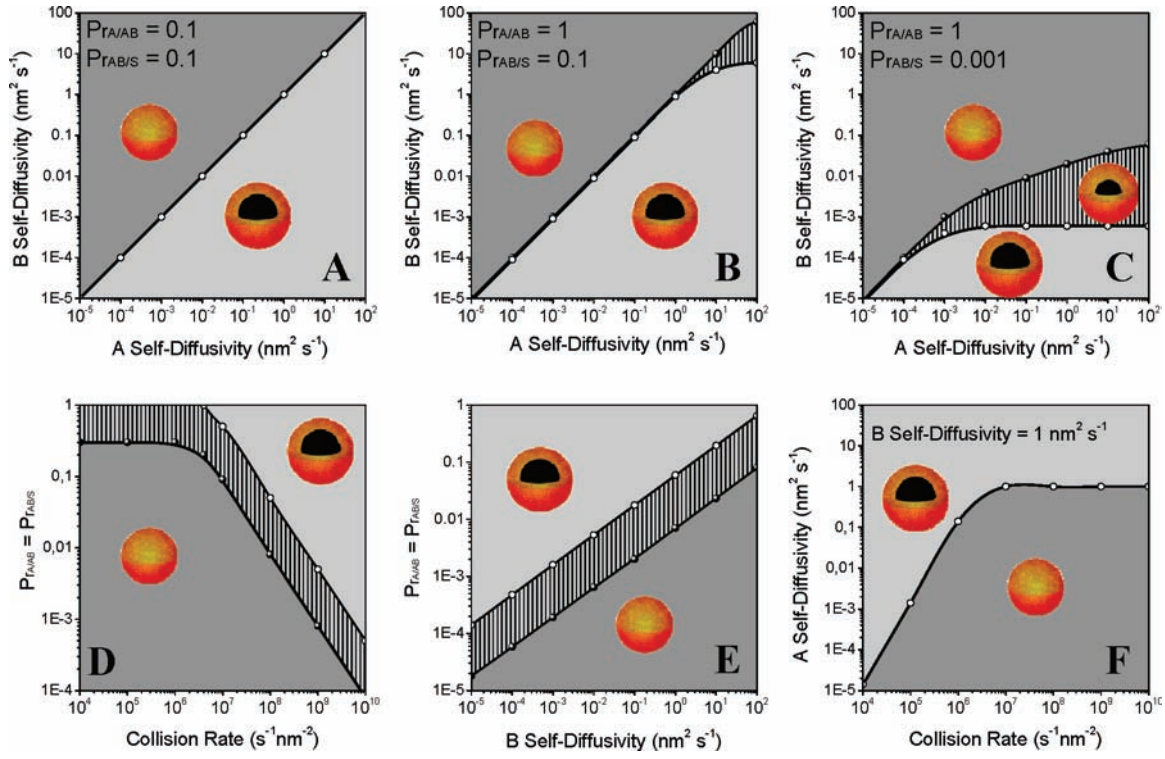

Figure 2. Phase diagrams for the particle geometry obtained from the reaction of A and B in different conditions. (A−C) Phase diagrams as a function of the A and B self-diffusivities for three different reaction rates and a collision frequency 10^8 s^{-1} nm^{-2}. (D) Phase diagram as a function of the collision rate and the reaction probabilities, which are considered equal at both interfaces. A and B self-diffusivities are 2 and 1 nm^2 s^{-1}, respectively. (E) Phase diagram as a function of the B self-diffusivity and the reaction probabilities, which are considered equal at both interfaces. The self-diffusivity of A is set to be 10 times larger than that of B, and the collision rate is 10^8 s^{-1} nm^{-2}. (F) Phase diagram as a function of the collision frequency and A self-diffusivity. Reaction probabilities are 1 at each interface, and B self-diffusivity is set to 1 nm^2 s^{-1}. Darker and lighter gray areas symbolize solid and completely hollow (complete outward growth of the shell, i.e., at the AB/S interface) structures, respectively. The intermediate regions symbolize an intermediate growth: the shell grows partially at the AB/S interface and partially at the A/AB interface. In the shaded parameter area, the resulting structures are hollow but do not have the highest inner-to-outer ratios possible.

the shell, which depends on the ion self-diffusivity and the shell thickness at each iteration, is smaller than the reaction time and 0 when the diffusion time is larger.

Figure 2 shows the phase diagrams of the particle geometry obtained from the iteration of these equations until the core element is totally consumed. For these simulations, an initial particle radius of 200 nm and the density and *FW* of CdSe are considered. In Figures 2A−C, the phase diagrams are shown as a function of the self-diffusivities for different reaction probabilities at each interface. The collision rate for graphs A−C and E is set to $I = 10^8$ s^{-1} nm^{-2}, which we estimate to approximate to our experimental conditions: [Se] $\sim 10^{-3}$ nm^{-3} and Se diffusion in solution $D_{Se} \sim 10^7$ nm^2 s^{-1}. Notice that in these conditions, for equal reaction probabilities at each interface, the shell growth is controlled by the ions self-diffusivities and hollow particles are obtained only if and when the self-diffusion is larger for A than B, as usually assumed. However, three other scenarios exist where the shell growth is not controlled by the ion self-diffusion, but by the reaction rate at each interface: (i) When the probability of reaction is higher at the A/AB than at the AB/solution interface, solid nanostructures can be formed even when the self-diffusivity in AB is larger for A than for B (Figure 2B and 2C). In this case, the shell growth is controlled by the reaction rate at the preferential reaction interface. (ii) Low reaction probabilities are associated with a slower rate of shell growth than of ion diffusion. In this regime, the ions diffuse and distribute homogeneously across the shell. Therefore, the reaction takes place in both fronts simultaneously, leading to the formation of solid particles even when the self-diffusivity through AB is larger for A than for B ions (Figure 2D and 2E). (iii) On the other hand, high reaction probabilities but low collision rates result in hollow particles even from reaction couples where the self-diffusivity through AB is larger for B than for A (Figure 2F). In this scenario, the reaction is limited by the availability of B at the particle surface, which also results in a slow shell growth rate and allows the eventually slower A ions to diffuse to the AB/solution interface. The AB/solution interface becomes constantly loaded with A ions that rapidly react with the impeding B molecules, preventing them from diffusing inside. In these conditions, all of the reaction takes place at the AB/solution interface, and hollow particles are formed.

These simulations provide an explanation for the experimental results obtained from the reaction of Cd particles with different S precursors and different Se concentrations. The very distinct reactivity of TOPS and DCB:S, reflected on the very different reaction times, places each reaction in a different regime, which explains the disparity in the final particle geometry obtained. While the reaction of Cd with DCB:S is limited by the self-diffusivity of the ions through the CdS shell,[4] the sulfidation of Cd with TOPS is controlled by the Cd-TOPS reaction rate. Moreover, we believe TOPS to preferentially react at the Cd/CdS interface. This preferential reaction front is evidenced when increasing the reaction rate by raising the reaction temperature. Above 300 °C the reaction of Cd with TOPS results in almost single-crystalline CdS structures having high aspect ratios (Figure 1D). The variable thickness through each rod indicates the reaction to take place at the Cd/CdS interface, thus producing an increasingly thinner rod as the Cd core is consumed. A very limited number of nucleation events occur, and just one or a few rods, up to 4 μm long, are formed from each Cd particle. Such occurrence can only be explained

considering a preferential reaction at the Cd/CdS interface instead of at the bare Cd surface or at the CdS/solution interface.

Unlike with TOPS, the reaction of Cd with large TOPSe concentrations results in hollow structures. The complete selenization of the Cd particles with large concentrations of TOPSe takes place in a much shorter time than its sulfidation with TOP:S due to the higher reactivity of the phosphine−Se complex. However, the relative low inner-to-outer radius ratios of the CdSe hollow particles obtained points toward shell growth taking place between a reaction and self-diffusion limited regimes. When reducing the TOPSe concentration in solution, we further shift the shell growth toward the reaction-limited regime, and solid particles are obtained. In this last case, the combination of a low collision rate and a relatively low reaction probability allows both ions to diffuse through the shell, resulting in a simultaneous reaction front at both interfaces.

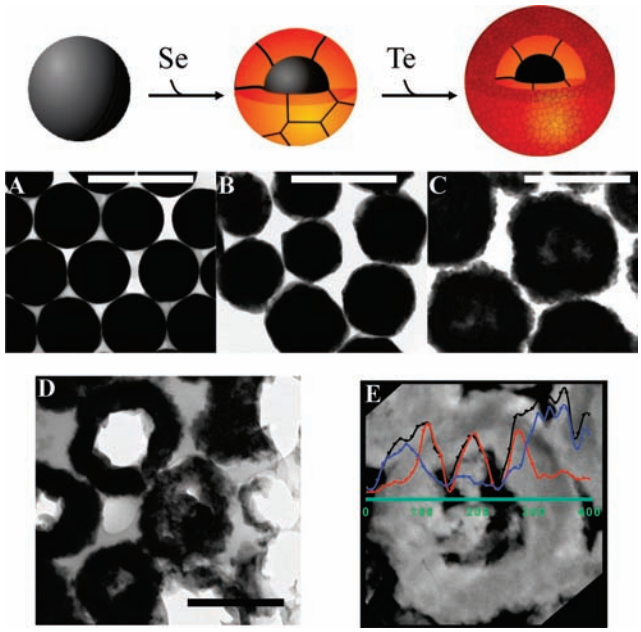

Figure 3. Scheme and TEM micrographs of the initial Cd particles (A); the Cd/CdSe core−shell particles (B); and the particles after a final reaction with TOPTe (C). The scale bar corresponds to 400 nm. (D) TEM micrograph of a slice of the fully reacted particles (scale bar = 400 nm). (E) EDX intensities as a function of the spatial position superimposed to a TEM micrograph of the analyzed particle cross section. The graph *x*-axis marks the analyzed line across the particle. Its scale is represented in nm. The color code of the EDX intensities is as follows: black = Cd; blue = Te; red = Se.

To confirm the self-diffusion of Cd through the formed CdSe not to be the limiting shell growth parameter, we injected TOPTe into a solution of partially reacted Cd/CdSe particles. Such Cd/CdSe particles were obtained from the reaction of Cd with a small concentration of Se and therefore consisted of core−shell particles with no detachment. The reactivity of the phosphine−Te complex is higher than that of TOPSe. From the reaction of TOPTe ([Te]/[Cd] = 1) with the Cd/CdSe core/shell particles, hollow particles were obtained (Figure 3). To characterize the final shell composition, the particles were embedded in a polymer, and slices of this composite were thinned down using the same preparation techniques used for TEM characterization of thin film cross sections. Figure 3D shows a TEM micrograph of the cross sections of representative hollow particles. Figure 3E shows the results of the nanoprobe EDX analysis superimposed upon the TEM micrograph of the probed particle cross section. Notice how the Te and Se concentration maxima are segregated. The EDX analyses reveal the composition of the external shell to be CdTe and that of the internal shell to be CdSe. We conclude that the Cd−Te reaction takes place at the CdSe/solution interface, illustrating that the Cd transport through CdSe takes place in a shorter time scale than the shell growth. Therefore, the CdSe shell growth obtained from the reaction of Cd with low TOPSe concentration is not limited by the Cd self-diffusion, but by the combination of a low collision frequency and the relatively low reactivity of TOPSe.

In conclusion, the formation of hollow vs solid AB particles from the reaction of A particles with a B precursor depends on the following main parameters: the differential of A and B self-diffusion rates through AB, the A−B reaction probabilities at each interface, and the interaction frequency of B with the particle, which is determined by the concentration and diffusivity of B in solution. The different combinations of these parameters lead to four shell growth regimes: (i) The self-diffusion limited regime, resulting in the formation of AB hollow particles only if and when the self-diffusion is larger for A than B in AB. Such is the case of the reaction of Cd with large concentrations of DCB:S. (ii) The preferential reaction regime, resulting in solid particles when the reaction probability at the A/AB interface is larger than that at the AB/solution interface. We believe such to be the case for the reaction of Cd with TOPS. (iii) The reaction-rate limited regime, where low reaction probabilities allow the ions to diffuse through the shell and react simultaneously at both interfaces to produce solid particles. This scenario is observed on the reaction of Cd with low concentrations of TOPSe. (iv) The collision-limited regime, where low interaction frequencies but large reaction probabilities allow A ions to diffuse and load the AB/solution interface, preventing the B ions to diffuse inside. The improved understanding of the reaction mechanism allows for further control of the Kirkendall effect synthetic route, offering the possibility to produce hollow particles with a broader range of homogeneous and even heterogeneous compositions.

Acknowledgment. This work was supported by the Director, Office of Science, Office of Basic Energy Sciences, of the U.S. Department of Energy under Contract No. DE-AC02-05CH11231. The authors acknowledge support of the National Center for Electron Microscopy at Lawrence Berkeley National Laboratory, which is also supported by the U.S. Department of Energy under Contract No. DE-AC02-05CH11231.

Note Added after ASAP Publication. The units for collision rate were incorrect in the version published ASAP July 24, 2009. The corrected version was published July 28, 2009.

Supporting Information Available: Detailed explanation of the kinetic model used, XRD and HRTEM of the CdS particles. This material is available free of charge via the Internet at http://pubs.acs.org.

References

(1) Yin, Y.; Rioux, R. M.; Erdonmez, C. K.; Hughes, S.; Somorjai, G. A.; Alivisatos, A. P. *Science* **2004**, *304*, 711.
(2) (a) Fan, H. J.; Gösele, U.; Zacharias, M. *Small* **2007**, *3*, 1660. (b) Cabot, A.; Puntes, V. F.; Shevchenko, E.; Yin, Y.; Balcells, L.; Marcus, M. A.; Hughes, S. M.; Alivisatos, A. P. *J. Am. Chem. Soc.* **2007**, *129*, 10358. (c) Liu, B.; Zeng, H. C. *J. Am. Chem. Soc.* **2004**, *126*, 16744. (d) Chiang, R.-K.; Chiang, R.-T. *Inorg. Chem.* **2007**, *46*, 369.
(3) Yin, Y.; Erdonmez, C. K.; Cabot, A.; Hughes, S.; Alivisatos, A. P. *Adv. Funct. Mater.* **2006**, *16*, 1389.
(4) Cabot, A.; Smith, R. K.; Yin, Y.; Zheng, H.; Reinhard, B. M.; Liu, H.; Alivisatos, A. P. *ACS Nano* **2008**, *2*, 1452.
(5) The CdS (CdSe) shell growth rates were calculated by monitoring the appearance of CdS (CdSe) with a concomitant decrease in the Cd in aliquots removed at successive times after the precursor injection. X-ray diffraction was used to quantitatively measure the fraction of CdS (CdSe) over Cd.

JA903751P